Environ Earth Sci (2010) 61:821–836
DOI 10.1007/s12665-009-0394-9

ORIGINAL ARTICLE

Comparison of landslide susceptibility mapping methodologies for Koyulhisar, Turkey: conditional probability, logistic regression, artificial neural networks, and support vector machine

Işık Yilmaz

Received: 25 June 2009 / Accepted: 21 November 2009 / Published online: 9 December 2009

Abstract This case study presented herein compares the GIS-based landslide susceptibility mapping methods such as conditional probability (CP), logistic regression (LR), artificial neural networks (ANNs) and support vector machine (SVM) applied in Koyulhisar (Sivas, Turkey). Digital elevation model was first constructed using GIS software. Landslide-related factors such as geology, faults, drainage system, topographical elevation, slope angle, slope aspect, topographic wetness index, stream power index, normalized difference vegetation index, distance from settlements and roads were used in the landslide susceptibility analyses. In the last stage of the analyses, landslide susceptibility maps were produced from ANN, CP, LR, SVM models, and they were then compared by means of their validations. However, area under curve values obtained from all four methodologies showed that the map obtained from ANN model looks like more accurate than the other models, accuracies of all models can be evaluated relatively similar. The results also showed that the CP is a simple method in landslide susceptibility mapping and highly compatible with GIS operating features. Susceptibility maps can be easily produced using CP, because input process, calculation and output processes are very simple in CP model when compared with the other methods considered in this study.

Keywords Landslide · Susceptibility map · GIS · Conditional probability · Logistic regression · Artificial neural networks · Support vector machine

I. Yilmaz (✉)
Department of Geological Engineering, Faculty of Engineering, Cumhuriyet University, 58140 Sivas, Turkey
e-mail: iyilmaz@cumhuriyet.edu.tr

Introduction

Natural disasters such as hurricanes, earthquakes, erosion, tsunamis, and landslides cause the loss of human life and damages to properties, and landslide can be accepted as one of very important natural disasters worldwide. If engineering geological data are presented in a hazard map form, they will be very useful tool for engineers for their urban planning. As reported by Popescu (1996), in order to define the landslide problem, it is an essential prerequisite to establish realistic landslide-prone zones and depict these zones on maps, which in turn will allow an effective land management.

Landslide susceptibility mapping before the landslide assessment is very important for safe planning, disaster management, and hazard mitigation. Creation of the susceptibility map will reduce these losses (Ayala 1987; Coraminas 1987; Chacón et al. 1992, 1994, 1996). A number of different models have been developed in order to assess landslide susceptibility, and these maps were produced by use of deterministic and non-deterministic (probabilistic) models. The probabilistic models are more frequently used, and a large number of methodologies have been developed (Rengers et al. 1998), based on the inventory of landslides, geomorphological analysis, qualitative and statistical bivariate analysis (Brabb et al. 1972; DeGraff and Romesburg 1980; Jade and Sarkar 1993; Irigaray 1995; Chung and Fabbri 1999; Fernández et al. 2003; Yilmaz and Yildirim 2006; Yilmaz 2008), and multivariate analysis (Carrara et al. 1991; Baeza 1994; Chung et al. 1995). Many researchers have used different techniques such as heuristic approach (Ives and Messerli 1981; Rupke et al. 1988; Barredo et al. 2000; Van Westen et al. 2000; Van Westen and Lulie 2003), deterministic models (Ward et al. 1982; Cascini et al. 1991; Gokceoglu and Aksoy 1996), and statistical methods (Van Westen 1993; Chacón et al. 1994, 1996; Chung and Fabbri 1999; Dai et al. 2001; Lee and Min 2001; Carrara et al. 2003; Yilmaz 2008).

Because of the deficiencies centered around the pore water pressure development in the soils and their spatial and temporal distribution, some physically based models had been developed and produced by researchers. Well-known physically based approaches for assessing slope stability and hazards had been developed by Hammond et al. (1992), Montgomery and Dietrich (1994), and Pack et al. (1998).

Some other techniques such as fuzzy-logic, artificial neural network (ANN), neuro-fuzzy model, etc. were used in assessment of the landslide susceptibility because of some limitations such as insufficient knowledge about the area of interest, which sometimes leads to unacceptable generalizations, reproducibility of the results and the subjectivity of the weighting of variables, high degree of oversimplification when the data are incomplete, prohibitive data requirements in deterministic models, etc. Several papers dealing with fuzzy-logic such as Juang et al. (1992), Davis and Keller (1997), Binaghi et al. (1998), Gorsevski et al. (2003), Tangestani (2003), and Ercanoglu and Gokceoglu (2004) were published. ANN had also been used to produce map showing landslide susceptibility in several papers such as Lu and Rosembaum (2003), Lee et al. (2003, 2004), Gomez and Kavzoglu (2005), Yesilnacar and Topal (2005), Yilmaz and Keskin (2007), and Yilmaz (2008, 2009a).

In this paper, landslide susceptibility maps of Koyulhisar (Sivas, Turkey) were prepared by use of ANNs, conditional probability (CP), logistic regression (LR), and support vector machine (SVM) models. At the end of the study, the maps obtained from four models were then compared according to their validation degrees. This paper will also add an extra value to the literature of the landslide susceptibility mapping as a comparative study of very basic technique (CP) with both statistical (LR) and soft computing techniques (ANN, SVM).

Study area and landslides

Koyulhisar is located on a slope of hilly region 130 km NE of Sivas (Turkey) (Fig. 1). It is constructed in the side of a mountain and the region is frequently subjected to landslides (Fig. 2). Koyulhisar is highly mountainous and wooded, and subjected to many landslides. The highest hills are Boztepe (1,361 m asl), Saytepe (1,240 m asl) and Igdir Mountain (1,850 m asl). Slope angle in the study area varies from 0° to 88°. The study area enclosing a rectangle of $\sim$131.6 km^2 is located in the North Anatolian Fault Zone (NAFZ) (Fig. 1) and affected by faulting. The main fault in the study area is the North Anatolian Fault which extends NW–SE. The other three faults are Dumanlica, Şıhlar, and Çamlıyaka (Fig. 2). The rocks in the study area are intensively fractured, and a number of joint sets (up to 4) dissecting the rock masses into small blocks are observed. The extension of the joints ranges from a few centimeters to tens of meters (Sendir and Yilmaz 2002).

The rocks outcropping (Fig. 2) in the landslide area consist of Pliocene volcanics, Eocene Yesilce Formation, and limestones of Maestrihtien age. These rocks are covered by younger colluviums composed of loose materials detached from bedrock. Thin-bedded, whitish yellow and pink, crushed and jointed limestone (Igdir formation) is the oldest unit in the study area. The Yesilce Formation described by Terlemez and Yılmaz (1980) consists of conglomerates, sandy-gravelly limestone, andesite, basalt, and pyroclastics. Jointed and massive Erdembaba volcanics comprises dacite, andesite, and basalts. Slopes in the study

Fig. 1 Study area in Turkey

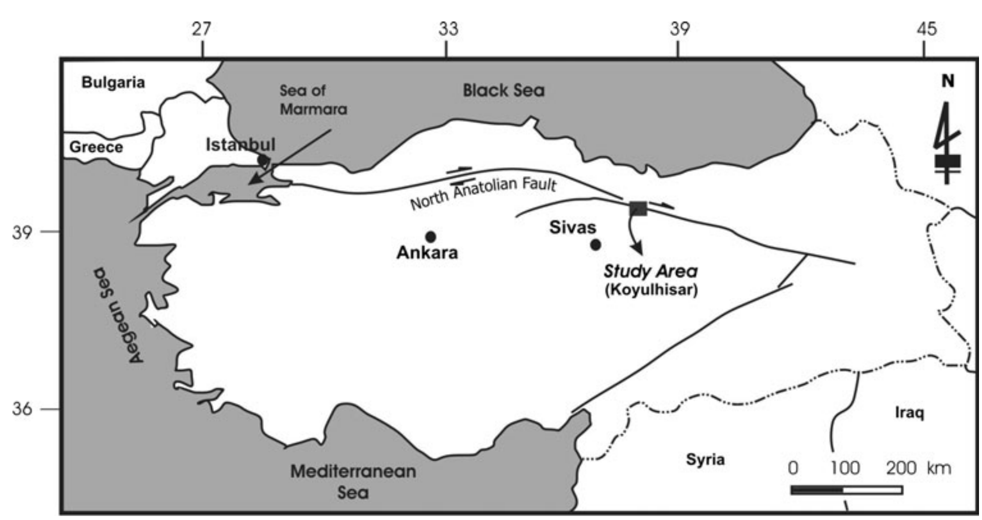

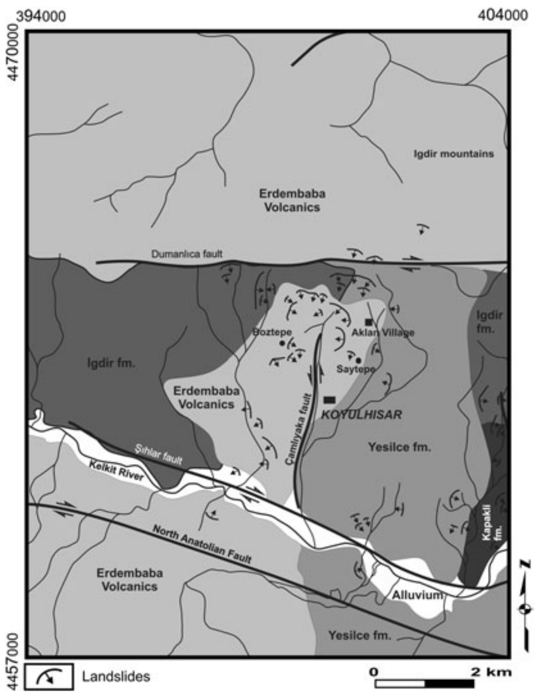

Fig. 2 Geological map of the study area (Sendir and Yilmaz 2002)

area are partly covered by soil material having a thickness of 50 cm to 2–3 m (Sendir and Yilmaz 2002).

Landslides generally occur after wet winter season, causing a movement throughout northern Koyulhisar (Sendir and Yilmaz 2002; Yilmaz et al. 2006). Forests, properties, roads, and agricultural lands had been damaged by the two large landslides occurred on 19 August 1998 and 20 June 2000.

The first landslide affected an area of 1.5 km^2, and has an approximate volume of 400,000 m^3. Aklan creek which is approximately 2 km away from Koyulhisar was fully filled by debris of landslide material within 24 h, as a consequence of landslides occurred in a direction of NE–SW in the hills of Aklan village of Koyulhisar (Sivas). The settlements in Koyulhisar were threatened by landslide, and Saytepe hill (in the north of Koyulhisar) provided a barrier to protect the settlements from the landslide. Movements remained stable in 2 days, and new tension cracks started to appear at the back of the main scarp. The main tension crack extended and reached about 150 m in length and 1–1.5 m in width.

On 20 June 2000, a new crack was observed in the slope 250–300 m above the previous landslide. The movement subsequently accelerated, and the whole area was involved in a renewed movement during the morning of 21 June 2000. The movement resulted in destruction of some houses. The new movement was accompanied by the appearance of tension cracks at the top of the slope. This landslide was directly related to rainfall. The continuous monitoring of the slide area from 19 August 1998 until 15 May 2000 had shown a total movement of approximately 2.5 m.

The mechanism of landslides can be explained as series progressive landslides occurred after the rainstorms. The deep-seated elements of 49 landslides affecting a total area of ~ 1 km^2 involve rotational sliding surface, and they contain many local slides (Fig. 3). Each local slide leads to the removal of the lateral support of the block's upslope, and progressively worsens the stability of the system. Otherwise, a rotational slide starts first and the removal of the lateral supports induces the slides upslope. So, many daylights of slides and ground movements through slope material are observed in sliding mass (Fig. 3). Another type of the stability problem is observed as flow of the cover, which is formed of particularly weak soils, on the rock mass. Flows following the topographic gradient occur generally in the rainy conditions. These types of mass movements in the study area occur in the shallow top soil horizons.

Wooded characteristics of the study area control the rate of runoff. The trees on the slopes slow down the surface flow of water, sourced from rain and melted snow, and make the infiltration into the earth material of the slopes easy. Thus, adding the weight to the slope and increasing of the pore water pressure contribute to the landslide. Movement of Koyulhisar slide was also caused by reactivation of the

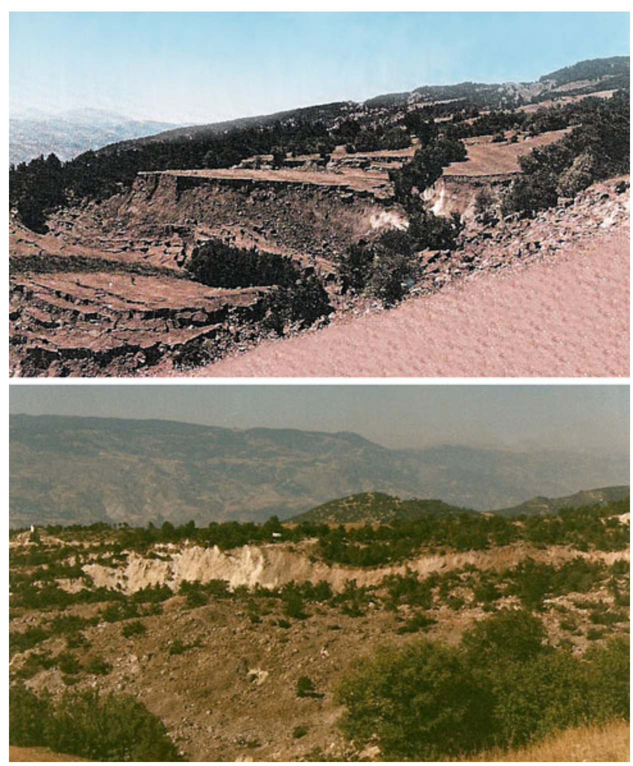

Fig. 3 Photos of landslides occurred in 19 August 1998

pre-existing slides or activation of recent slides. Highly fractured rock material resulting from old landslide in conjunction with an unfavorable tectonic situation sets the stage for the large movement that took place (Sendir and Yilmaz 2002; Yilmaz et al. 2006).

Shallow to very deep landslides are observed in the study area. In order to obtain landslide susceptibility map, very few shallow flow type slides were eliminated in the analysis.

Rainfall is the main significant source of water in the study area, and it is the most important element in the hydrologic cycle. Study area receives a mean annual rainfall of 394.6 mm. The minimum recorded rainfall was ~266 mm in 1962 and the maximum was ~575 mm in 1983. Most rainfall occurs during May, with a mean value of 64.4 mm. The mean maximum temperature in August is 20.6°C; the mean minimum temperature is always recorded in January as −1.9°C. It is declared by the populace in Koyulhisar that the study area received the most rainfall of the last 20 years before the last two landslide events.

Construction of spatial data base

In the study area, landslides larger than one cell (10×10 m^2) were used in the analyses. In the landslide inventory mapping, for each landslide, the main scarp was distinguished from the accumulation/depletion zone or rupture zone as polygon feature drawn (Yilmaz 2009b) from Landsat TM satellite images (May 2006, Scene ID: 17432), 1:35,000 aerial photographs, and field works (Fig. 4).

Digital elevation model (DEM) (Fig. 5) having a ground resolution of 10 m was constructed by implementation of 1:25,000 scaled topographical map contours using ArcMap of ArcGIS 9.1 software. The maps of the landslide-related factors such as geological (lithology and distance from faults) (Fig. 6), topographical (slope angle and aspect; topographical elevation; distance from drainage; topographic wetness index, TWI; stream power index, SPI) (Fig. 7) and environmental (the normalized difference vegetation index, NDVI; distance from roads and settlements) (Fig. 8) parameters were then obtained.

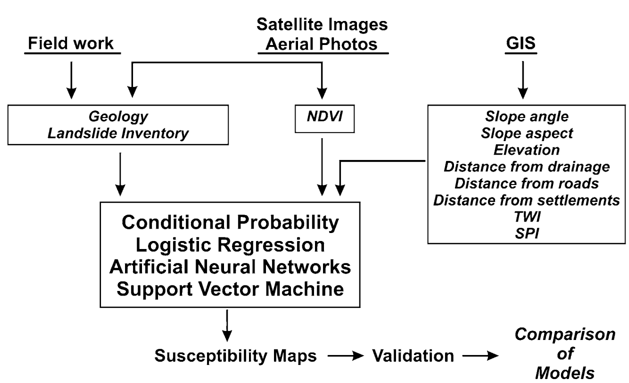

Fig. 4 Flowchart of the works for production of landslide susceptibility maps

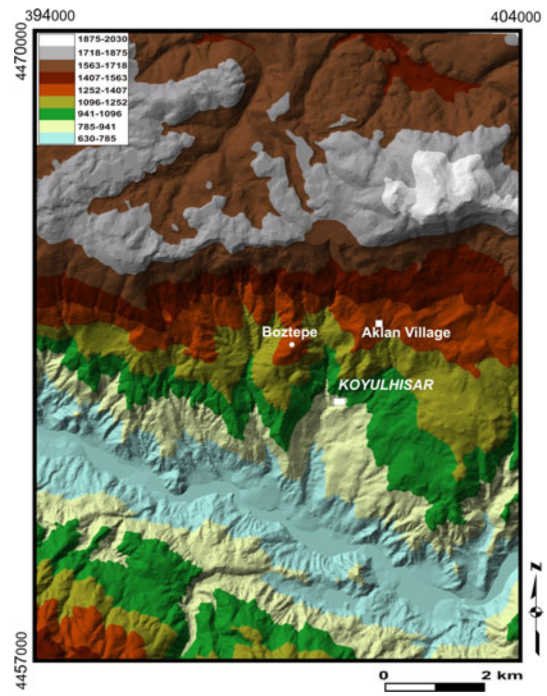

Fig. 5 Digital elevation model (DEM) of the study area

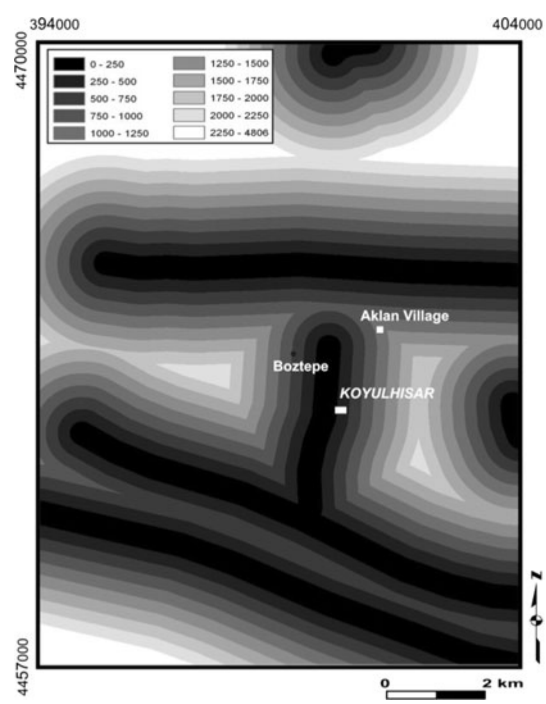

Fig. 6 Landslide affecting factor of distance from faults

Proximity to the structural elements is a very important contributing parameter in the evaluation of landslide susceptibility. That is why distances to faults were calculated at 250 m intervals by buffering (Fig. 6). It was observed that landslides occur in Kapakli, Igdir, and Yesilce formations, and probability of landslide occurrence increases with decreasing of distance from faults.

Analyses showed that slope angle in a range of 14°–56° (Fig. 7a) indicates high probability of landslide occurrence. As a general aspect, shear stresses on the slope material increase with increasing slope degree; it is expected that landslides will occur on the steepest slopes. On the other hand, very low shear stresses are expected at gentle slopes. Analyses related to slope as a contributing factor showed that the low probability of landslide occurrence obtained in the areas having a steeper slope more than 56°. Because, steeper slopes than 56° are generally not susceptible to shallow landslides due to the bedrock outcrops and their eroded characteristics. Slope aspect analyses (Fig. 7b) showed that landslides were most abundant in E, S, SE, SW facing slopes. Relationships between elevation and landslide occurrence indicated that landslides generally occur at the elevation range of 1,080–1,530 m. It can be seen from Figs. 1 and 7e that landslides are also very rare at higher elevation than 1,530 m, and this sparseness is sourced from very thin soil cover and rocky characteristics of the areas at higher elevations (Fig. 7c). In order to assess the influence of drainage on the landslide occurrence, distance from drainage was calculated at 150 m intervals (Fig. 7d). At the distance closer to the drainage system, a high probability of landslide occurrence was found.

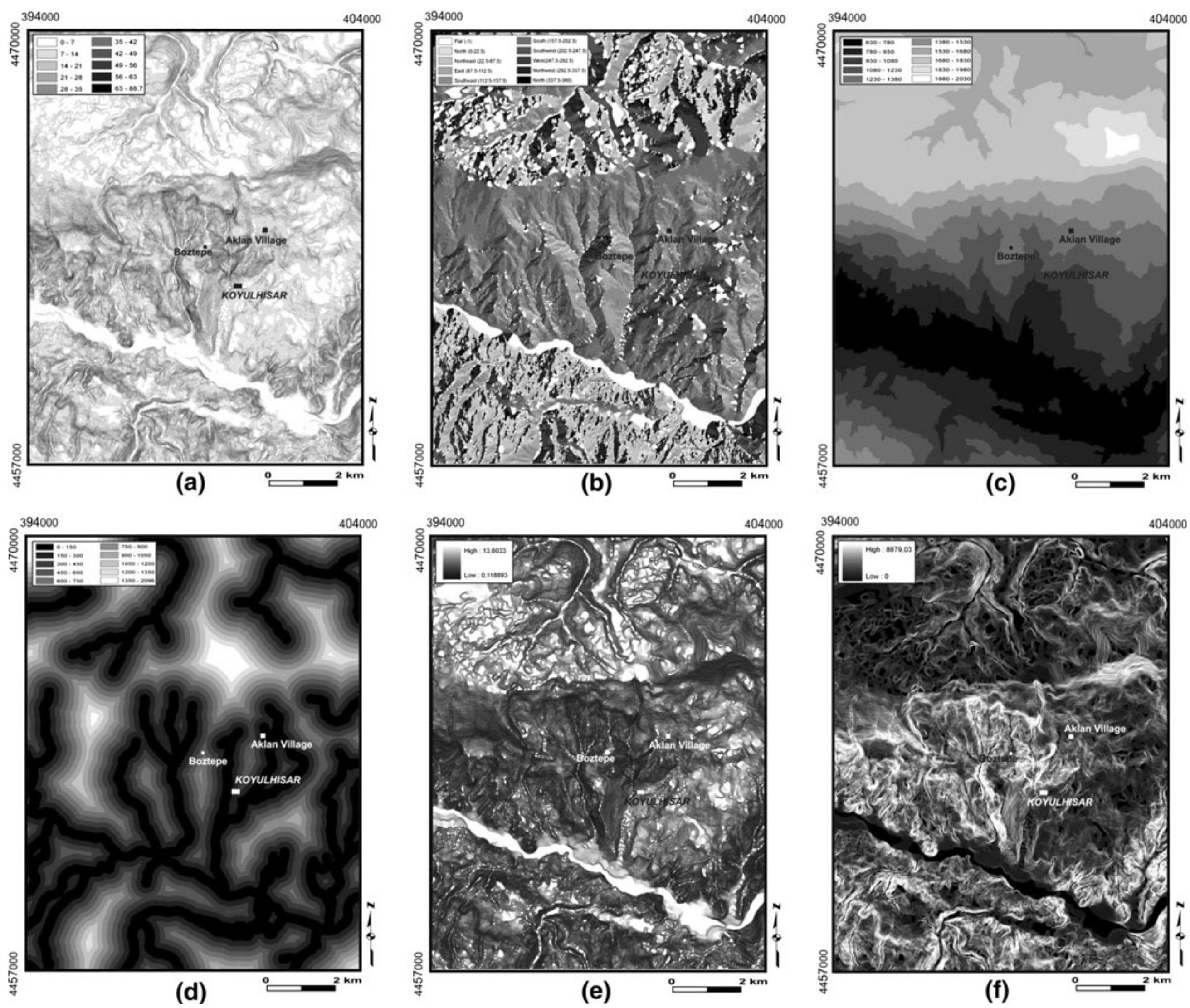

Fig. 7 Landslide affecting topographical factor maps of **a** slope gradient, **b** slope aspect, **c** elevation, **d** distance from drainage, **e** topographical wetness index (TWI), and **f** stream power index (SPI)

Topography firstly controls the spatial variation of hydrological conditions and slope stabilities. It affects the spatial distribution of soil moisture, and groundwater flow often follows surface topography (Burt and Butcher 1986; Seibert et al. 1997; Rodhe and Seibert 1999; Zinko et al. 2005). Topographic indices have, therefore, been used to describe the spatial soil moisture patterns (Burt and Butcher 1986; Moore et al. 1991). One such index is the TWI developed by Beven and Kirkby (1979) within the runoff model. It is defined as

$$\mathrm{TWI} = \ln(a/\tan\beta) \tag{1}$$

where a is the local upslope area draining through a certain point per unit contour length and $\tan\beta$ is the local slope. The TWI has been used to study spatial scale effects on hydrological processes. Water infiltration to slope material causes pore water pressures and decreases the soil strength. In this study, TWI (Fig. 7e) was taken under consideration as a contributing factor. In this analysis, a transmissivity value of 1 was used constant for the whole catchments area.

Higher TWI values, distributed in higher elevations, point out the infiltration of surface water into the slope forming materials, and pore water pressures increase with decreasing shear strength. It was observed that landslides were very abundant at the lower elevations than locations having high TWI values at higher locations.

As another topographical index, the SPI (Fig. 7f), which is a measure of erosive power of the stream, was computed for the study area. SPI can be defined by the following equation:

$$\mathrm{SPI} = A_s \tan\beta \tag{2}$$

where A_s is the specific catchment area and β is the local slope gradient in degrees.

NDVI is a measure of surface reflectance and gives a quantitative estimate of the vegetation growth and biomass (Hall et al. 1995). Satellite maps of vegetation show the density of plant growth over the entire globe. The most common measurement is called the NDVI. Very low values of NDVI (0.1 and below) correspond to barren areas, sand, or snow. Moderate values represent shrub and grassland (0.2–0.3), while high values indicate temperate and tropical rainforests (0.6–0.8) (Weier and Herring 2005).

Using the satellite image of Landsat Thematic Mapper (TM), the NDVI (Fig. 8a) was taken into the consideration as a landslide-related factor. The NDVI was calculated from the following formula:

$$\mathrm{NDVI} = (\mathrm{IR} - \mathrm{R})/(\mathrm{IR} + \mathrm{R}) \tag{3}$$

where IR is the infrared portion of the electromagnetic spectrum, R is the red portion of the electromagnetic spectrum.

The results of NDVI analyses showed that the landslides focused into the grassland areas and afforested areas. The maps of distance from roads (Fig. 8b) and settlement areas (Fig. 8c) were also constructed by buffering having the respective intervals of 250 and 400 m. It was found that frequency of the landslides occurrence decreases with increasing of the proximity to the both of roads and settlement areas.

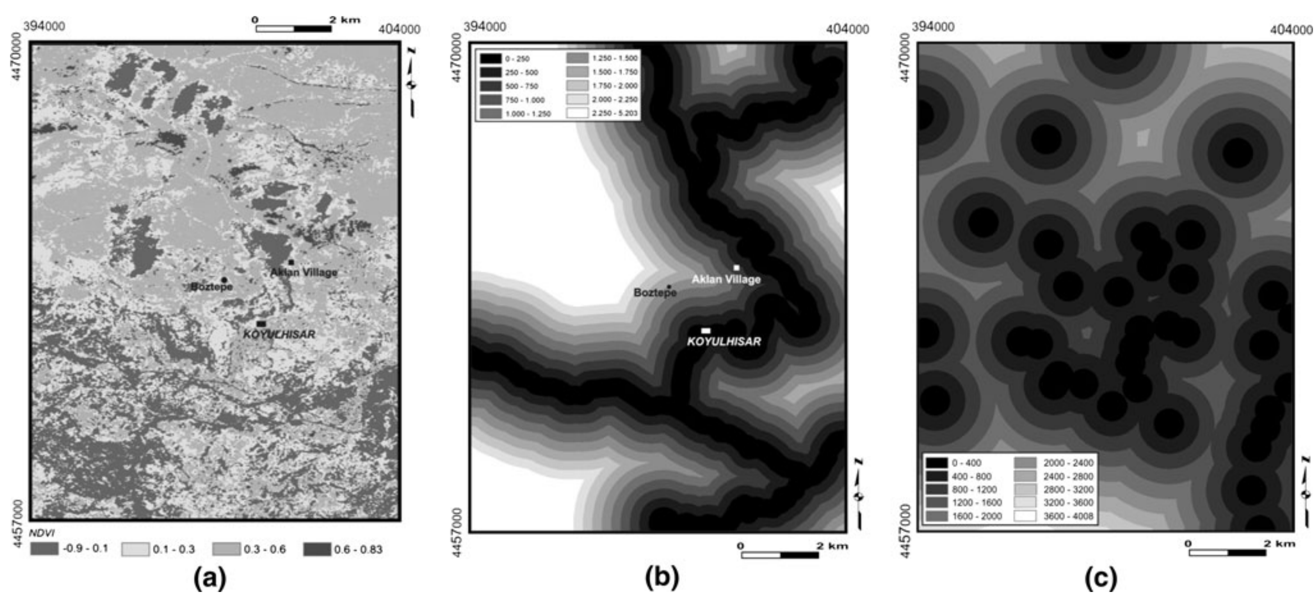

Fig. 8 Landslide affecting environmental factor maps of **a** normalized difference vegetation index (NDVI), **b** distance from main roads, and **c** distance from settlements

The relationships between landslides and factors were first explained using frequency ratio (Table 1), and factors were selected according to their importance in order to use in the analyses. All factor maps and landslide inventory were then entered into GIS medium using ArcGIS 9.1 (2005) software.

Landslide susceptibility mapping

CP model

Conditional probability is a simple method for producing landslide susceptibility map and highly compatible with GIS. Number of factors related to landslide occurrences can be considered in the CP approach. The data layers containing each factor subdivided into a convenient number of classes are crossed in order to obtain possible combinations of the various classes of the different factors (Clerici et al. 2002).

Each specific combination represents a pixel, and the landslide spatial frequency is subsequently determined within each pixel. The resulting landslide density equals the landslide susceptibility, assuming that the slope failure in future will be more likely occurred under those conditions which led to the past instability and frequency of an event equals the probability that the same event will occur (Clerici et al. 2002). CP is denoted mathematically as P(A|B) (Eq. 4) (Negnevitsky 2002):

$$P(\mathrm{A}|\mathrm{B}) = (\text{the number of times A and B can occur})/(\text{the number of times B can occur}) \quad (4)$$

The number of times A and B can occur, or the probability that both A and B will occur, is also called “joint probability” of A and B. It represents mathematically as $P(\mathrm{A}\cap\mathrm{B})$. The number of ways B can occur is the probability of B, P(B):

$$P(\mathrm{A}|\mathrm{B}) = P(\mathrm{A}\cap\mathrm{B})/P(\mathrm{B}) \quad (5)$$

$$P(\mathrm{B}|\mathrm{A}) = P(\mathrm{B}\cap\ \mathrm{A})/P(\mathrm{A}) \quad (6)$$

$$P(\mathrm{B}\cap\mathrm{A}) = P(\mathrm{B}|\mathrm{A})\times P(\mathrm{A}) \quad (7)$$

$$P(\mathrm{A}\cap\mathrm{B}) = P(\mathrm{B}\cap\mathrm{A}) \quad (8)$$

Bayesian rule is given in Eq. 9, and Eq. 10 can be written as event A being dependent on a number of mutually exclusive events B1, B2, …, Bn:

$$P(\mathrm{A}|\mathrm{B}) = [P(\mathrm{B}|\mathrm{A})\times P(\mathrm{A})]/P(\mathrm{B}) \quad (9)$$

$$P(\mathrm{A}) = \sum_{i=1}^{n} P(\mathrm{A}\cap\mathrm{B}) = \sum_{i=1}^{n} P(\mathrm{A}|\mathrm{B}_i)P(\mathrm{B}_i) \quad (10)$$

Landslide susceptibility maps were produced using Eq. 10 (Fig. 9a) within map algebra in GIS environment, and the P(A|B), P(A) and P(B) values are tabulated in Table 2.

The values of landslide susceptibility index (LSI) were classified using equal areas. The proportions are sorted from the smallest to the largest. This range of values is broken into five groups to represent the relative susceptibility in the study area. To ensure that the points used to define the five groups are determined objectively, a non-hierarchical cluster analysis is used (Yilmaz 2007).

An initial division into five groups is achieved by breaking equally the range of proportional values present. The upper and lower boundaries of each group are retained or adjusted to ensure that the final division represents the minimum sum of the squared deviations around the four group means. This is based on the W function (Anderberg 1973).

LR model

Multiple regression analysis is the most common statistical method used in earth sciences, and expressed as a linear equation below:

$$Y = b_0 + b_1x_1 + b_2x_2 + \cdots + b_nx_n \quad (11)$$

where Y is the dependent variable representing the presence (1) or absence (0), b_0 the intercept of model, b_1, …, b_n the partial regression coefficients, x_1, …, x_n the independent variables.

At the beginning of the analysis, a map showing the area affected by landslides and factor maps in raster format were converted into ASCII format. Statistical software (SPSS 10.0) was then used to estimate the correlation between landslide event and landslide affecting factors. An equation predicting the landslide occurrence was obtained as following:

$$\begin{aligned} Y = {} & 5.992 + (\mathrm{GEOL}^{(*)}) + (-0.01342\times\mathrm{FAULT}) \\ & + (0.0488\times\mathrm{SLOPE}) + (\mathrm{ASPECT}^{(*)}) \\ & + (-0.0191\times\mathrm{ELEV}) + (-0.0177\times\mathrm{DRAIN}) \\ & + (0.0302\times\mathrm{TWI}) + (-0.0229\times\mathrm{SPI}) \\ & + (-0.00541\times\mathrm{NDVI}) \\ & + (-0.0226\times\mathrm{ROAD}) + (-0.0198\times\mathrm{SETTL}) \end{aligned} \quad (12)$$

for (*), see Table 3.

In order to predict the possibility of landslide occurrence in each grid, probability was calculated from:

$$p = \frac{1}{1+e^{-Y}} \quad (13)$$

Finally, susceptibility map was obtained by converting the file into the raster format (Fig. 9b).

Table 1 Frequency ratios for factors (LSA: landslide affected grid; grid: grids in domain)

Class	LSA (%) (a)	Grid (%) (b)	FR (a)/(b)	Class	LSA (%) (a)	Grid (%) (b)	FR (a)/(b)
Slope				Distance from settlements			
0–7	5.17	21.04	0.25	0–400	28.86	12.01	2.40
7–14	20.01	26.56	0.75	400–800	50.81	22.89	2.22
14–21	22.94	23.30	0.98	800–1,200	14.20	21.62	0.66
21–28	22.02	15.35	1.43	1,200–1,600	5.79	17.31	0.33
28–35	15.81	8.86	1.79	2,000–2,400	0.00	10.24	0.00
35–42	11.83	3.76	3.14	2,400–2,800	0.00	5.79	0.00
42–49	1.87	0.61	3.09	2,800–3,200	0.00	3.34	0.00
49–56	0.28	0.10	2.77	3,200–3,600	0.00	2.12	0.00
56–63	0.05	0.07	0.72	4,000–4,400	0.00	1.26	0.00
63–89	0.01	0.34	0.03	>4,400	0.00	0.37	0.00
Distance from fault				Aspect			
0–250	10.03	13.29	0.75	Flat	1.84	13.33	0.14
250–500	32.56	13.30	2.45	N	0.53	5.44	0.10
500–750	26.46	12.59	2.10	NE	4.86	9.17	0.53
750–1,000	15.10	10.03	1.51	E	13.47	8.86	1.52
1,000–1,250	4.48	9.32	0.48	SE	19.09	10.70	1.78
1,250–1,500	3.82	8.91	0.43	S	28.32	16.34	1.73
1,500–1,750	7.54	8.10	0.93	SW	16.72	13.87	1.21
1,750–2,000	0.01	6.50	0.00	W	10.85	9.27	1.17
2,000–2,250	0.00	5.82	0.00	NW	3.81	8.12	0.47
>2,250	0.00	12.14	0.00	N	0.51	4.91	0.10
Distance from drainage				TWI			
0–150	25.32	22.80	1.11	0.11–1.38	38.07	21.90	1.74
150–300	30.77	20.49	1.50	1.39–1.85	31.81	27.20	1.17
300–450	21.14	15.86	1.33	1.86–2.33	16.41	22.77	0.72
450–600	11.07	10.73	1.03	2.34–2.81	9.58	14.94	0.64
600–750	9.33	9.09	1.03	2.82–2.39	3.66	7.00	0.52
750–900	2.36	6.77	0.35	2.40–4.07	0.22	2.68	0.08
900–1,050	0.01	5.81	0.00	4.08–4.98	0.18	2.26	0.08
1,050–1,200	0.00	4.03	0.00	4.99–6.14	0.04	0.57	0.07
1,200–1,350	0.00	2.27	0.00	6.15–7.83	0.02	0.47	0.05
>1,350	0.00	2.15	0.00	7.84–13.60	0.00	0.21	0.00
Topographical elevation				SPI			
630–780	9.16	14.58	0.63	0–750	5.88	22.75	0.26
780–930	12.07	12.76	0.95	750–1,500	22.69	28.64	0.79
930–1,080	7.93	11.34	0.70	1,500–2,250	25.33	23.42	1.08
1,080–1,230	17.80	9.14	1.95	2,250–3,000	20.99	14.63	1.43
1,230–1,380	22.32	7.30	3.06	3,000–3,750	17.01	7.41	2.30
1,380–1,530	20.08	5.37	3.74	3,750–4,500	7.18	2.30	3.12
1,530–1,680	9.89	14.26	0.69	4,500–5,250	0.78	0.31	2.50
1,680–1,830	0.74	21.49	0.03	5,250–6,000	0.11	0.07	1.43
1,830–1,980	0.00	2.77	0.00	6,000–6,750	0.03	0.17	0.19
>1,980	0.00	0.99	0.00	>6,750	0.00	0.29	0.00
Distance from roads				NDVI			
0–250	9.73	15.61	0.62	−0.9 to 0.1	33.84	31.52	1.07
250–500	22.01	11.64	1.89	0.1–0.3	21.55	23.48	0.92
500–750	13.74	9.01	1.53	0.3–0.6	43.08	39.64	1.09

Table 1 continued

Class	LSA (%) (a)	Grid (%) (b)	FR (a)/(b)	Class	LSA (%) (a)	Grid (%) (b)	FR (a)/(b)
750–1,000	18.38	12.92	1.42	0.6–0.83	1.53	5.36	0.29
1,000–1,250	10.89	7.80	1.40	Geology			
1,250–1,500	12.71	8.61	1.48	Kapaklı fm.	6.55	2.23	2.94
1,500–1,750	5.97	5.42	1.10	Alluvium	0.88	4.24	0.21
1,750–2,000	4.62	4.27	1.08	Volcanics	40.76	60.37	0.68
2,000–2,250	1.96	3.68	0.53	Igdir fm.	25.99	14.78	1.76
>2,250	0.00	21.05	0.00	Yesilce fm.	25.81	18.38	1.40

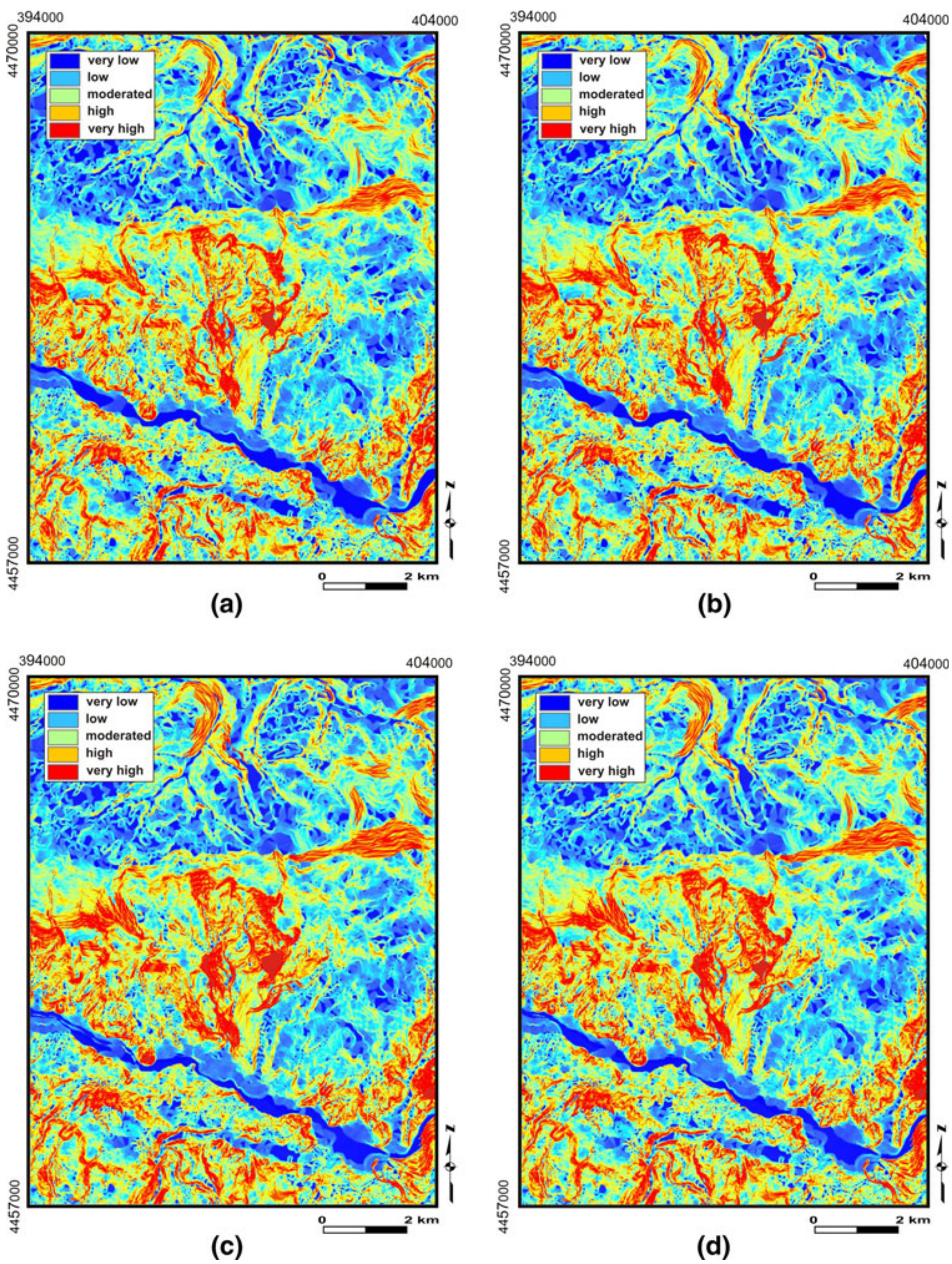

Fig. 9 Landslide susceptibility map produced from conditional probability (CP) (**a**), logistic regression (LR) (**b**), artificial neural networks (ANN) (**c**), and support vector machine (SVM) (**d**) models

Table 2 Results of the $P(A/B_i)$ obtained from the conditional probability model

Class	P(A)	$P(B_i)$	$P(A/B_i)$	Class	P(A)	$P(B_i)$	$P(A/B_i)$
Slope				Distance from settlements			
0–7	0.000369	0.2104	0.001756	0–400	0.002063	0.120138	0.017168
7–14	0.00143	0.2656	0.005384	400–800	0.003631	0.228925	0.015862
14–21	0.001639	0.233	0.007036	800–1,200	0.001015	0.216216	0.004692
21–28	0.001574	0.1535	0.010251	1,200–1,600	0.000413	0.173075	0.002389
28–35	0.00113	0.0886	0.012751	2,000–2,400	0	0.102356	0
35–42	0,000845	0.0376	0.022483	2,400–2,800	0	0.057884	0
42–49	0.000134	0.0061	0.021906	2,800–3,200	0	0.033403	0
49–56	2E−05	0.001	0.020009	3,200–3,600	0	0.021165	0
56–63	3.57E−06	0.0007	0.005104	4,000–4,400	0	0.012641	0
63–89	7.15E−07	0.0034	0.00021	>4,400	0	0.003747	0
Distance from fault				Aspect			
0–250	0.000717	0.1329	0.005393	Flat	0.000131	0.1333	0.000986
250–500	0.002327	0.133	0.017494	N	3.79E−05	0.0544	0.000696
500–750	0.001891	0.1259	0.015018	NE	0.000347	0.0917	0.003787
750–1,000	0.001079	0.1003	0.010758	E	0.000963	0.0886	0.010864
1,000–1,250	0.00032	0.0932	0.003435	SE	0.001364	0.107	0.012749
1,250–1,500	0.000273	0.0891	0.003064	S	0.002024	0.1634	0.012385
1,500–1,750	0.000539	0.081	0.006652	SW	0.001195	0.1387	0.008614
1,750–2,000	7.15E−07	0.065	1.1E−05	W	0.000775	0.0927	0.008364
2,000–2,250	0	0.0582	0	NW	0.000272	0.0812	0.003353
>2,250	0	0.1214	0	N	3.64E−05	0.0491	0.000742
Distance from drainage				TWI			
0–150	0.001809	0.228	0.007936	0.11–1.38	0.00272	0.219	0.012422
150–300	0.002199	0.2049	0.010731	1.39–1.85	0.002273	0.272	0.008357
300–450	0.001511	0.1586	0.009525	1.86–2.33	0.001173	0.2277	0.00515
450–600	0.000791	0.1073	0.007372	2.34–2.81	0.000685	0.1494	0.004582
600–750	0.000667	0.0909	0.007335	2.82–2.39	0.000262	0.07	0.003736
750–900	0.000169	0.0677	0.002491	2.40–4.07	1.57E−05	0.0268	0.000587
900–1,050	7.15E−07	0.0581	1.23E−05	4.08–4.98	1.29E−05	0.0226	0.000569
1,050–1,200	0	0.0403	0	4.99–6.14	2.86E−06	0.0057	0.000501
1,200–1,350	0	0.0227	0	6.15–7.83	1.43E−06	0.0047	0.000304
>1,350	0	0.0215	0	7.84–13.60	0	0.0021	0
Topographical elevation				SPI			
630–780	0.000655	0.1458	0.00449	0–750	0.00042	0.2275	0.001847
780–930	0.000863	0.1276	0.00676	750–1,500	0.001621	0.2864	0.005661
930–1,080	0.000567	0.1134	0.004997	1,500–2,250	0.00181	0.2342	0.007729
1,080–1,230	0.001272	0.0914	0.013917	2,250–3,000	0.0015	0.1463	0.010252
1,230–1,380	0.001595	0.073	0.021849	3,000–3,750	0.001216	0.0741	0.016404
1,380–1,530	0.001435	0.0537	0.026721	3,750–4,500	0.000513	0.023	0.022308
1,530–1,680	0.000707	0.1426	0.004956	4,500–5,250	5.57E−05	0.0031	0.01798
1,680–1,830	5.29E−05	0.2149	0.000246	5,250–6,000	7.86E−06	0.0007	0.011229
1,830–1,980	0	0.0277	0	6,000–6,750	2.14E−06	0.0017	0.001261
>1,980	0	0.0099	0	>6,750	0	0.0029	0
Distance from roads				NDVI			
0–250	0.000695	0.1561	0.004454	−0.9 to 0.1	0.002418	0.3152	0.007672
250–500	0.001573	0.1164	0.013512	0.1–0.3	0.00154	0.2348	0.006559
500–750	0.000982	0.0901	0.010897	0.3–0.6	0.003078	0.3964	0.007766

Table 2 continued

Class	P(A)	P(B$_i$)	P(A/B$_i$)	Class	P(A)	P(B$_i$)	P(A/B$_i$)
750–1,000	0.001313	0.1292	0.010166	0.6–0.83	0.000109	0.0536	0.00204
1,000–1,250	0.000778	0.078	0.009977	Geology			
1,250–1,500	0.000908	0.0861	0.010549	Kapaklı fm.	0.000468	0.0223	0.020989
1,500–1,750	0.000427	0.0542	0.007871	Alluvium	6.29E−05	0.0424	0.001483
1,750–2,000	0.00033	0.0427	0.007732	Volcanics	0.002913	0.6037	0.004825
2,000–2,250	0.00014	0.0368	0.003806	Igdir fm.	0.001857	0.1478	0.012566
>2,250	0	0.2105	0	Yesilce fm.	0.001844	0.1838	0.010035

Table 3 Logistic regression coefficients of categorical data

Category	Coefficient
Geological	
Kapakli formation	0.012392
Alluvium	−0.000123
Volcanics	−0.000231
Igdir formation	0.009234
Yesilce formation	0.007812
Slope aspect	
Flat	−0.000141
N	−0.000237
NE	−0.000326
E	0.008912
SE	0.009271
S	0.007931
SW	0.006734
W	0.006112
NW	−0.000316
N	−0.000237

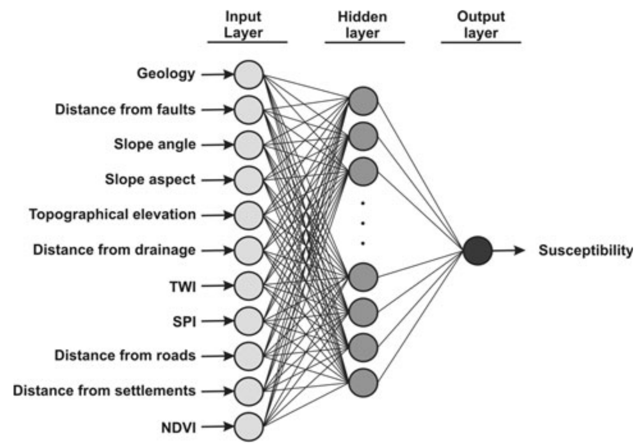

Fig. 10 Neural network structure used in the study

ANN model

As stated by Gomez and Kavzoglu (2005), an alternative method for landslide susceptibility zonation is the use of ANNs. ANNs are an attempt, in the simplest way, to imitate the neural system of the human brain. Neural networks may be used as a direct substitute for autocorrelation, multivariable regression, linear regression, trigonometric and other statistical analysis and techniques (Singh et al. 2003). Neural networks, with their remarkable ability to derive meaning from complicated or imprecise data, can be used to extract patterns and detect trends that are too complex to be noticed by either humans or other computer techniques. ANNs have the ability to handle imprecise and fuzzy data they can work with continuous, categorical and binary data without violating any assumptions. As assessment of probability for landsliding is performed through the forecast of future events from experience of past landslides, it may be considered an ideal application for ANNs.

Neural networks consist of a large class of different architectures. In many cases, the issue is approximating a static nonlinear, mapping $f(\mathbf{x})$ with a neural network $f(\mathbf{x})_{\mathrm{NN}}$, where $\mathbf{x} \in \mathbf{R^K}$. There are many kinds of ANN models, among which the backpropagation (BP) model is the most widely used, and it is an instructive training model. It is accepted that the most useful neural networks in prediction and decision algorithm are BP and radial basis function (RBF) networks. In this paper, BP algorithm created by generalizing the Widrow–Hoff learning rule to multiple layer networks and nonlinear differentiable transfer function is used. A BP consists of an input layer, several hidden layers, and output layers. All of those layers may contain multiple nodes (Yilmaz and Yüksek 2008a, b).

MatLab 7.0 was used for training and testing the neural networks. A three-layer feed-forward network that consists of an input layer (11 neurons), one hidden layer (23 neurons) and one output layer was used as a network structure of 10-23-1 (Fig. 10). In order to find the number of hidden layer nodes, Eq. 14 proposed by Hecht-Nielsen (1987) was used:

$$N_{\mathrm{h}} = 2N_{\mathrm{i}} + 1 \quad (14)$$

Table 4 Weights of each factor

Factors	Weights
Geology	1.67316
Slope gradient	2.87173
Slope aspect	1.21121
Elevation	2.01342
Topographical wetness index	1.99321
Stream power index	1.73927
Distance from faults	1.99899
Distance from drainage	1.62133
Distance from roads	2.21132
Distance from settlements	1.91137
Normalized difference vegetation index	1.49978

where N_i is the number of input nodes and N_h is the number of hidden nodes.

Initial weight range is also an important parameter influencing the convergence of learning rule. In this study, weights were randomly initialized in a small range of −0.25 to 0.25 as proposed by Kavzoglu (2001). Kavzoglu (2001) has also suggested that the minimum number of training samples should be more than $30N_i(N_i + 1)$ where N_i is the number of input nodes. Learning and momentum parameters were set as follows as proposed by Foody et al. (1996). Almost 21,000 pixels were randomly selected from the two classes (landslide and non-landslide) as training samples, and parameters were then adjusted as below.

Learning parameters: 0.1.
Momentum parameters: 0.9.
Networks training function: variable learning rate with momentum (traingdx).
Activation (transfer) function for all layers: tansig.

Moreover, training areas were checked in the field for accuracy and completeness. As in many other network training methods, models and parameters were used to be able to reach minimum root mean square error (RMSE) values. RMSE goal for stopping criterion was set to 0.1. After the network goal was reached, the whole study area was fed into the network in order to estimate the landslide susceptibility. The learning algorithm defines how network weights are adjusted between successive training cycles or epochs. Using the BP learning algorithm which operates by searching an error surface defined as a function of weights, using a gradient descent technique to locate the point (weight combination) with minimum error. The weights for minimum error were recorded in the analyses, and weights of each factor can be seen in Table 4. The set of susceptibility values obtained in each grid were then converted to raster file in GIS medium, and landslide susceptibility map was produced (Fig. 9c).

SVM model

As concluded by Bai et al. (2008), nowadays, the data-driven models are becoming more important, and particularly machine learning methods provide promising perspectives in the landslide susceptibility mapping, being well-suited to nonlinear high-dimensional data modeling problems.

SVM is a more recently developed method that is based on nonlinear transformations of the covariates into a higher dimensional feature space (Brenning 2005). SVM is an increasingly popular learning procedure based on statistical learning theory, and involves a training phase in which the model is trained by a training dataset of associated input and target output values. The trained model is then used to evaluate a separate set of testing data. There are two main ideas underlying the SVM for discriminant-type problems. The first is an optimum linear separating hyperplane that separates the data patterns. The second is the use of kernel functions to convert the original nonlinear data patterns into the format that is linearly separable in a high-dimensional feature space (Yao et al. 2008).

Two class SVM model is described by Yao et al. (2008) as following.

A set of linear separable training vectors x_i ($i = 1, 2, \ldots, n$) consist of two classes, which are denoted as $y_i = \pm 1$. The goal of the SVM is to search for an n-dimensional hyperplane differentiating the two classes by the maximum gap.

Mathematically, it can be minimized

$$\frac{1}{2}\|w\|^2 \tag{15}$$

Subject to the following constrains

$$y_i((w \cdot x_i) + b) \geq 1 \tag{16}$$

where $\|w\|$ is the norm of the normal of the hyperplane, b is a scalar base, and $(\cdot)$ denotes the scalar product operation. Introducing the Lagrangian multiplier, the cost function can be defined as

$$L = \frac{1}{2}\|w\|^2 - \sum_{i=1}^{n} \lambda_i (y_i((wx_i) + b) - 1) \tag{17}$$

where λ_i is the Lagrangian multiplier. The solution can be achieved by dual minimizing Eq. 17 with respect to w and b through the standard procedures, and the detailed discussions can be found in Vapnik (1995) and Tax and Duin (2002) (Yao et al. 2008).

For non-separable case, one can modify the constraints by introducing slack variables ξ_i (Vapnik 1995):

$$y_i((wx_i) + b) \geq 1 - \xi_i \tag{18}$$

Equation 15 will be modified as

$$L = \frac{1}{2}\|w\|^2 - \frac{1}{\upsilon n}\sum_{i=1}^{n} \xi_i \quad (19)$$

where $\upsilon(0, 1]$ is introduced to account for misclassification (Scholkopf et al. 2000; Hastie et al. 2001). In addition, a kernel function $K(x_i, x_j)$ is introduced by Vapnik (1995) to account for nonlinear decision boundary (Yao et al. 2008).

In this study, two-class SVM method was used, because Yao et al. (2008) had reported that the more accurate susceptibility map was produced from the two-class SVM. For this reason, in this study, RBF was employed for kernel and the two class SVM model was first trained and then used to construct landslide susceptibility map. In the study, +1 and −1 represent the failed and stable cases, respectively. One can easily note that stable cases are not available and they have to be generated. Landslide affecting parameter maps were represented by vector of real numbers in the SVM model used. Data sets and their classes are given in Table 2. Landslide susceptibility map produced by SVM model can be seen in Fig. 9d.

Validation of the models used

The landslide susceptibility maps can be tested using the known landslide locations. Validation was performed by comparing the known landslide location data, which were not included in the susceptibility analyses, with the susceptibility map obtained. The area under curve (AUC) is a good indicator to evaluate the prediction performance of the model and the largest AUC, varying from 0.5 to 1.0, is the most ideal model (Swets 1988; Yesilnacar and Topal 2005). After the calculated LSI values of all cells were sorted in descending orders, the ordered grid values of LSI were divided into 100 classes which were accumulated 1%. Cumulative percentage of landslide occurrence in the classes versus LSI curves was then drawn to calculate AUC (Fig. 11). The obtained values of AUC from the four mapping models are given in Fig. 9. Although ANN is the most accurate method, the results for all four used methodologies do not show significant difference, i.e., all four approaches lead to very similar results and, therefore, can be used in landslide susceptibility mapping.

Moreover, validation by field investigations was also performed by comparing the known landslide location data with the classes of landslide susceptibility in maps. The results obtained from field observation were also found to be harmonious with results of AUC.

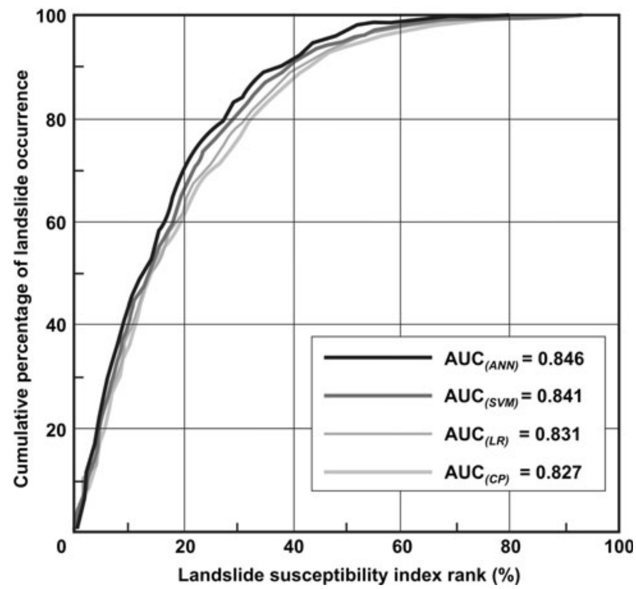

Fig. 11 Area under curve (AUC) representing the quality of the models used

Conclusions and recommendations

Landslide susceptibility can be assessed from different methods based on the GIS technology. Especially in the last years, many research papers were published in order to solve deficiencies and difficulties in assessment of the susceptibility. It should be aimed that the procedure for preparing landslide susceptibility map must be simple and have a higher accuracy (Yilmaz 2008, 2009a).

In this study, CP model as a simple method, LR, neural networks and SVM as complex methods were applied to construct landslide susceptibility maps. The results of this study showed that the map obtained from SVM and ANN models looks like having a better accuracy than the conventional statistical methods; however, all the models were found having relatively similar accuracies. Maps obtained from four models look the same with minor differences which can be distinguished in detail of the maps only. While the pixels represented by very low and low susceptibility in CP and LR model is more widespread than ANN and SVM, high and very high susceptible pixels are lesser than ANN and SVM. Sameness of the maps also supports the obtained similar accuracies of the models.

Yesilnacar and Topal (2005) stated that several investigators have compared neural network models with LR using different data sets, with some researchers finding superior performance for the neural networks and other authors finding no differences in overall predictive performance (Tu 1996; Schumacher et al. 1996; Ottenbacher et al. 2001; Mahiny and Turner 2003). They had also indicated that the susceptibility map produced from the neural networks model was found to be more realistic. Lee and Sambath (2006) reported in their comparative papers that the frequency ratio model (86.97%) and LR model (86.37%) showed higher and similar accuracy (Yilmaz 2009a, b).

Yao et al. (2008) presented the use of SVM in landslide susceptibility mapping, and they found that SVM is a useful tool in assessment of susceptibility. They also compared the resulting map to the map obtained from LR, and found better prediction efficiency than LR. Brenning (2005) also obtained sufficiently smooth prediction surfaces for creating susceptibility map by SVM.

The main problem in the use of ANN, LR, and SVM is time-consuming input process, calculations and output process. Because they require conversion of data used in analyses into ASCII or other formats, and it is also very hard to process the large amount of data in statistical software. That is why the CP model can be used as a simple tool in the assessment of landslide susceptibility and preparation of the maps. This paper has also a value with its comparative nature, because the use of conventional (CP, LR, etc.), soft computing (ANN, etc.) and machine learning method (SVM, etc.) in landslide susceptibility mapping was compared for the first time.

Acknowledgments Author thanks the two anonymous reviewers for their very constructive and valuable comments which significantly led to the improvement of the paper.

References

Anderberg MR (1973) Cluster analysis for applications. Academic Press, New York

ArcGIS (Version 9.1) (2005) Integrated GIS software. ESRI, CA

Ayala FJ (1987) Introducción a los riesgos geológicos (Introduction to geological risk). In: Ayala FJ (ed) Riesgos Geológicos (Geological risks). IGME (Instituto Geologico y Minero de Espana, Spain Institute of Geology and Mining), Serie Geología Ambiental, Madrid, Spain, pp 3–19

Baeza C (1994) Evaluación de las condiciones de rotura y la movilidad de los deslizamientos superficiales mediante el uso de técnicas de análisis multivariante (Evaluation of the failure conditions and mobility by using multivariate analysis in superficial media). Thesis (PhD). University Politechnique Catalunya (in Spanish)

Bai SB, Wang J, Lu GN, Kanevski M, Pozdnoukhov A (2008) GIS-based landslide susceptibility mapping with comparisons of results from machine learning methods process versus logistic regression in Bailongjiang river basin, China. Geophysical Research Abstracts, EGU, 10, A-06367

Barredo JJ, Benavides A, Hervas J, Van Westen CJ (2000) Comparing heuristic landslide hazard assessment techniques using GIS in the Trijana basin. Gran Canaria Island, Spain, JAG2 (1):9–23

Beven KJ, Kirkby MJ (1979) A physically based, variable contributing area model of basin hydrology. Hydrol Sci Bull 24:43–69

Binaghi E, Luzi L, Madella P, Rampini A (1998) Slope instability zonation: a comparison between certainty factor and fuzzy Dempster-Shafer approaches. Nat Hazards 17:77–97

Brabb EE, Pampeyan EH, Bonilla M (1972) Landslide susceptibility in the San Mateo County, California, scale 1:62,500. U.S.G.S. Miscellaneous Field Studies Map, MF344

Brenning A (2005) Spatial prediction models for landslide hazards: review, comparison and evaluation. Nat Hazards Earth System Sci 5:853–862

Burt T, Butcher D (1986) Stimulation from simulation–a teaching model of hillslope hydrology for use on microcomputers. J Geogr Higher Educ 10:23–39

Carrara A, Cardinalli M, Detti R, Guzzetti F, Pasqui V, Reichenbach P (1991) GIS techniques and statistical models in evaluating landslide hazards. Earth Surf Proc Land 16:427–445

Carrara A, Crosta G, Frattini P (2003) Geomorphological and historical data in assessing landslide hazard. Earth Surf Process Landform 28:1125–1142

Cascini L, Critelli S, Gulla G, Di Nocera S (1991) A methodological approach to landslide hazard assessment: a case history. In: Proceedings of 16th international landslide conference, Balkema, Rotterdam, pp 899–904

Chacon J, Irigaray C, Fenandez T (1992) Metodologia para la cartografia regianal de movientos de ladera y riesgos asociados mediante un Sistema de Informacions Geografica (Methodology in mapping of regional landslides by means of Geographical Information System). In: Corominas J, Alonso E (eds) III Simposio Nacional sobre Taludes y laderas Inesstables, La Corruna, Spain, I, pp 121–133

Chacón J, Irigaray C, Fernández T (1994) Large to middle scale landslide inventory, analysis and mapping with modeling and assessment of derived susceptibility, hazards and risks in a GIS. In: Proceedings of 7th IAEG congress, Balkema, Rotterdam, pp 4669–4678

Chacón J, Irigaray C, Fernández T (1996) From the inventory to the risk analysis: Improvements to a large scale GIS method. In: Chacón J, Irigaray C, Fernández T (eds) Proceedings of 8th international conference and field workshop on landslides, Balkema, pp 335–342

Chung CF, Fabbri AG (1999) Probabilistic prediction models for landslide hazard mapping. Photogramm Eng Remote Sens 65(12):1389–1399

Chung CF, Fabbri AG, van Westen CJ (1995) Multivariate regression analysis for landslide hazard zonation. In: Carrara A, Guzetti F (eds) Geographical informations systems in assessing natural hazards. Kluwer Publishers, Dordrecht

Clerici A, Perego S, Tellini C, Vescovi P (2002) A procedure for landslide susceptibility zonation by the conditional analysis method. Geomorphology 48:349–364

Coraminas J (1987) Criterios para la confeccion de mapes de peligrosidad de movimentos de ladera (Criteria for preparation of landslide hazard maps). In: Ayala FJ (ed) Riesgos Geologicos. IGME (Instituto Geologico y Minero de Espana, Spain Institute of Geology and Mining), Serie Geologia Ambiental, Madrid, Spain, pp 193–201

Dai FC, Lee CF, Zhang XH (2001) GIS-based geo-environmental evaluation for urban land-use planning: a case study. Eng Geol 61:257–271

Davis TJ, Keller CP (1997) Modeling uncertainty in natural resource analysis using fuzzy sets and Monte-Carlo simulation: slope instability prediction. Int J Geogr Inform Sci 11(5):409–434

DeGraff J, Romesburg H (1980) Regional landslide-susceptibility assessment for wildland management: a matrix approach. In: Coates D, Vitek J (eds) Thresholds in geomorphology. George Allen and Unwin, London, pp 401–414

Ercanoglu M, Gokceoglu C (2004) Use of fuzzy relations to produce landslide susceptibility map of a landslide prone area (West Black Sea Region Turkey). Eng Geol 75:229–250

Fernández T, Irigaray C, Hamdouni RE, Chacón J (2003) Methodology for landslide susceptibility mapping by means of a GIS. Application to the Contraviesa Area (Granada, Spain). Nat Hazards 30:297–308
Foody GM, Lucas RM, Curran PJ, Honzak M (1996) Estimation of the areal extend of land cover classes that only occur at a sub-pixel level. Can J Remote Sens 22:432–438
Gokceoglu C, Aksoy H (1996) Landslide susceptibility mapping of the slopes in the residual soils of the Mengen region (Turkey) by deterministic stability analyses and image processing technique. Eng Geol 44:147–161
Gomez H, Kavzoglu T (2005) Assessment of shallow landslide susceptibility using artificial neural networks in Jabonosa River Basin, Venezuela. Eng Geol 78(1–2):11–27
Gorsevski PV, Gessler PE, Jankowski P (2003) Integrating a fuzzy *k*-means classification and a Bayesian approach for spatial prediction of landslide hazard. J Geogr Syst 5(3):223–251
Hall FG, Townshend JR, Engman ET (1995) Status of remote sensing algorithms for estimation of land surface state parameters. Remote Sens Environ 51:138–156
Hammond C, Hall D, Miller S, Swetik P (1992) Level I Stability Analysis (LISA) Documentation Version 2.0. General Technical Report INT-285. United States Department of Agriculture, Forest Service Intermountain Research Station, USA
Hastie T, Tibshirani R, Friedman J (2001) The elements of statistical learning: data mining inference and prediction. Springer, New York
Hecht-Nielsen R (1987) Kolmogorov's mapping neural network existence theorem. In: Proceedings of 1st IEEE international conference on neural networks, San Diego, CA, USA, pp 11–14
Irigaray C (1995) Movimientos de ladera: inventoria, analisis y cartografaa de susceptibilidad mediante un Sistema de Informacion Geografica. Aplicacion a las zonas de Colmenar (Ma), Rute (Co) y Montefrio (Gr) (Landslides: inventory, susceptibility analysis and mapping by means of a Geographical Information System. Application to the Colmenar (Malaga), Rute (Cordoba) and Montefrio (Granada) sectors). Thesis (PhD). University Granada (in Spanish)
Ives JD, Messerli B (1981) Mountain hazard mapping in Nepal: introduction to an applied mountain research project. Mt Res Dev 1(3–4):223–230
Jade S, Sarkar S (1993) Statistical models for slope instability classification. Eng Geol 36:91–98
Juang CH, Lee DH, Sheu C (1992) Mapping slope failure potential using fuzzy sets. J Geotech Eng ASCE 118(3):475–493
Kavzoglu T (2001) An investigation of the design and use of feed-forward artificial neural networks in the classification of remotely sensed images. Thesis (PhD). University of Nottingham, School of Geography, 306 pp
Lee S, Min K (2001) Statistical analyses of landslide susceptibility at Yongin, Korea. Environ Geol 40:1095–1113
Lee S, Sambath T (2006) Landslide susceptibility mapping in the Damrei Romel area, Cambodia using frequency ratio and logistic regression models. Environ Geol 50(6):847–856
Lee S, Ryu JH, Min K, Won JS (2003) Landslide susceptibility analysis using GIS and artificial neural network. Earth Surf Proc Land 28(12):1361–1376
Lee S, Ryu JH, Won JS, Park HJ (2004) Determination and application of the weights for landslide susceptibility mapping using an artificial neural network. Eng Geol 71:289–302
Lu P, Rosembaum MS (2003) Artificial neural networks and grey systems for the prediction of slope instability. Nat Hazards 30(3):383–398
Mahiny AS, Turner BJ (2003) Modeling past vegetation change through remote sensing and GIS: a comparison of neural networks and logistic regression methods. In: Proceedings of the 7th international conference on geocomputation. University of Southampton, UK
Montgomery DR, Dietrich WE (1994) A physically based model for the topographic control on shallow landsliding. Water Resour Res 30(4):1153–1171
Moore ID, Grayson RB, Ladson AR (1991) Digital terrain modeling—a review of hydro- hydrological, geomorphological, and biological applications. Hydrol Process 5:3–30
Negnevitsky M (2002) Artificial intelligence—a guide to intelligent systems. Addison-Wesley Co., Great Britain, p 394
Ottenbacher KJ, Smith PM, Illig SB, Linn RT, Fiedler RC, Granger CV (2001) Comparison of logistic regression and neural networks to predict rehospitalization in patients with stroke. J Clin Epidemiol 54:1159–1165
Pack RT, Tarboton DG, Goodwin CN (1998) Terrain stability mapping with SINMAP, technical description and users guide for version 1.00. Report Number 4114-0. Terratech Consulting Ltd., Salmon Arm, BC, Canada (www.tclbc.com)
Popescu M (1996) From landslide causes to landslide remediation. In: Proceedings of 7th international symposium on landslides, Trondheim, Norway, pp 75–96
Rengers N, van Westen CJ, Chacón J, Irigaray C (1998) Draft for the chapter on the application of digital techniques for natural hazard zonation. Report on mapping of natural hazards. International Association of Engineering Geology. Commission no. 1 on Engineering Geological Mapping
Rodhe A, Seibert J (1999) Wetland occurrence in relation to topography: a test of topographic indices as moisture indicators. Agric For Meteorol 98–99:325–340
Rupke J, Cammeraat E, Seijmonsbergen AC, Van Westen CJ (1988) Engineering geomorphology of the Widentobel catchment, Switzerland: a geomorphological inventory system applied to geotechnical appraisal of the slope stability. Eng Geol 26:33–68
Scholkopf B, Smola A, Williamson RC, Bartlett PL (2000) New support vector algorithms. Neural Comput 12:1207–1245
Schumacher M, Robner R, Vach W (1996) Neural networks and logistic regression. Part I. Comput Stat Data Anal 21:661–682
Seibert J, Bishop KH, Nyberg L (1997) A test of TOPMODEL's ability to predict spatially distributed groundwater levels. Hydrol Process 11:1131–1144
Sendir H, Yilmaz I (2002) Structural, geomorphological and geomechanical aspects of the Koyulhisar landslides in the North Anatolian Fault Zone (Sivas-Turkey). Env Geol 42(1):52–60
Singh TN, Kanchan R, Verma AK, Singh S (2003) An intelligent approach for prediction of triaxial properties using unconfined uniaxial strength. Min Eng J 5(4):12–16
Swets JA (1988) Measuring the accuracy of diagnostic systems. Science 240:1285–1293
Tangestani MH (2003) Landslide susceptibility mapping using fuzzy gamma operation in a GIS, Kakan catchment area, Iran. Map India 2003, Disaster Management, 7 pp
Tax D, Duin E (2002) Uniform object generation for optimizing one-class classifiers. J Mach Learn Res 2:155–173
Terlemez İ, Yılmaz A (1980) Ünye-Ordu-Reşadiye-Koyulhisar-Karaçayır-Hafik arasında kalan bölgenin jeolojisi. M.T.A. Report No. 6671 (in Turkish)
Tu JV (1996) Advantages and disadvantages of using artificial neural networks versus logistic regression for predicting medical outcomes. J Clin Epidemiol 49(11):1225–1231
Van Westen CJ (1993) Application of geographic information systems to landslide hazard zonation. Thesis (PhD). Technical University Delft, ITC publication number 15, ITC, Enschede, The Netherlands, 245 pp
Van Westen CJ, Lulie GF (2003) Analyzing the evolution of the Tessina landslide using aerial photographs and digital elevation models. Geomorphology 54(1–2):77–89

Van Westen CJ, Soeters R, Sijmons K (2000) Digital geomorphological landslide hazard mapping of the Alpago area, Italy. Int J Appl Earth Observ Geoinform 2(1):51–59

Vapnik V (1995) Nature of statistical learning theory. Wiley, New York

Ward TJ, Ruh-Ming L, Simons DB (1982) Mapping landslide hazard in forest watershed. J Geotech Eng Div ASCE 108(GT-2):319–324

Weier J, Herring D (2005) Measuring vegetation (NDVI and EVI). Earth Observatory Library of NASA. http://earthobservatory.nasa.gov/Library/MeasuringVegetation/

Yao X, Tham LG, Dai FC (2008) Landslide susceptibility mapping based on support vector machine: a case study on natural slopes of Hong Kong, China. Geomorphology 101:572–582

Yesilnacar E, Topal T (2005) Landslide susceptibility mapping: a comparison of logistic regression and neural networks method in a medium scale study, Hendek region (Turkey). Eng Geol 79:251–266

Yilmaz I (2007) GIS based susceptibility mapping of karst depression in gypsum: a case study from Sivas basin (Turkey). Eng Geol 90:89–103

Yilmaz I (2008) A case study from Koyulhisar (Sivas-Turkey) for landslide susceptibility mapping by artificial neural networks. Bull Eng Geol Environ 68(3):297–306

Yilmaz I (2009a) Landslide susceptibility using frequency ratio, logistic regression, artificial neural networks and their comparison: a case study from Kat landslides (Tokat-Turkey). Comput Geosci 35(6):1125–1138

Yilmaz I (2009b) The effect of the sampling strategies on the landslide susceptibility mapping by conditional probability (CP) and artificial neural networks (ANN). Environ Earth Sci. doi: 10.1007/s12665-009-0191-5

Yilmaz I, Keskin I (2007) Sebinkarahisar ve Alucra yöresi heyelanları: Heyelan duyarlılık haritalarının Frekans Oranı (FR) ve Yapay Sinir Ağları (ANN) Modelleri kullanılarak hazırlanması. Cumhuriyet University BAP Project Report, M-342, 90 pp (in Turkish with English abstract)

Yilmaz I, Yildirim M (2006) Structural and geomorphological aspects of the Kat landslides (Tokat-Turkey), and susceptibility mapping by means of GIS. Env Geol 50(4):461–472

Yilmaz I, Yüksek AG (2008a) An example of artificial neural network application for indirect estimation of rock parameters. Rock Mech Rock Eng 41(5):781–795

Yilmaz I, Yüksek AG (2008b) Prediction of the strength and elasticity modulus of gypsum using multiple regression, ANN, ANFIS models and their comparison. Int J Rock Mech Min Sci 46(4):803–810

Yilmaz I, Ekemen T, Yıldırım M, Keskin I, Özdemir G (2006) Failure and flow development of a collapse induced complex landslide: the 2005 Kuzulu (Koyulhisar-Turkey) landslide hazard. Env Geol 49(3):467–476

Zinko U, Seibert J, Dynesius M, Nilsson C (2005) Plant species numbers predicted by a topography based groundwater-flow index. Ecosystems 8:430–441